Prediction of the shape of inline wave force and free surface elevation using First Order Reliability Method (FORM)

Ghadirian, Amin; Bredmose, Henrik; Schløer, Signe

Published in:
Energy Procedia

Link to article, DOI:
10.1016/j.egypro.2017.10.343

Publication date:
2017

Document Version
Publisher's PDF, also known as Version of record

Available online at www.sciencedirect.com

ScienceDirect

Energy Procedia 137 (2017) 162–176

Energy Procedia

www.elsevier.com/locate/procedia

14th Deep Sea Offshore Wind R&D Conference, EERA DeepWind'2017, 18-20 January 2017, Trondheim, Norway

Prediction of the shape of inline wave force and free surface elevation using First Order Reliability Method (FORM)

Amin Ghadirian[a,*], Henrik Bredmose[a], Signe Schløer[a]

[a]*DTU Wind Energy, Nils Koppels Alle Building 403, DK-2800 Kgs. Lyngby, Denmark*

Abstract

In design of substructures for offshore wind turbines, the extreme wave loads which are of interest in Ultimate Limit States are often estimated by choosing extreme events from linear random sea states and replacing them by either stream function wave theory or the NewWave theory of a certain design wave height. As these wave theories suffer from limitations such as symmetry around the crest, other methods to estimate the wave loads are needed. In the present paper, the First Order Reliability Method, FORM, is used systematically to estimate the most likely extreme wave shapes. Two parameters of maximum crest height and maximum inline force are used to define the extreme events. FORM is applied to first and second-order irregular waves in both 2D and 3D. The application is validated against the NewWave model and also the NewForce model, which is introduced as the force equivalent of NewWave theory, that is, the most likely time history of inline force around a force peak of given value. The results of FORM and NewForce are linearly identical and show only minor deviations at second order. The FORM results are then compared to wave averaged measurements of the same criteria for crest height and peak force value. Relatively good agreement between the FORM results of free surface elevation including the second order effects, and the wave averaged measurements is observed. However, the inline force time series reproduced using the numerical method are not as consistent with the measurements as the free surface elevation time series. The discrepancies between the FORM results and the measurements is found to be a result of more nonlinearity in the selected events than second order and negligence of the drag forces above still water level in the present analysis. This paper is one step toward more precise prediction of extreme wave shape and loads. Ultimately such waves can be used in the design process of offshore structures. The approach can be generalized to fully nonlinear models.

Peer-review under responsibility of SINTEF Energi AS.

Keywords: Extreme wave ; FORM; First Order Reliability Method; NewWave; NewForce;

1. Introduction

In the design process of offshore substructures, including but not limited to wind turbine monopiles, Ultimate Limit States (ULS) are significantly important. Given a design wave height, the extreme wave loads are often estimated by choosing extreme events from linear random sea states and replacing them by either non-linear regular waves (stream function wave theory [1]) or the NewWave theory [2] combined with a stretching method as suggested in the design

* Corresponding author.
E-mail address: amgh@dtu.dk

1876-6102
Peer-review under responsibility of SINTEF Energi AS.
10.1016/j.egypro.2017.10.343

codes [3]. Both of these theories are associated with limitations, the most important of which is the symmetry of these waves around the wave crest.

To avoid such shortcomings and to estimate a more realistic extreme wave, other theories and methods are suggested. One such method the "designer" wave approach by Grice et. al. [4]. This wave is the average shape of waves that can create an extreme event of choice. Another approach to find an extreme wave event is using the First Order Reliability Method (FORM) to calculate the shape of the most probable extreme waves which exceeds a certain maximum crest height or inline force.

FORM and its inverse process IFORM is used extensively in probabilistic design. In the Wind Energy industry IFORM is used as an extrapolation technique for extreme waves with 50 years return period. This is described in the Annex G of the design code of offshore wind turbines, IEC 61400-3 [3]. Based on such method Agarwal [5] used IFORM to extrapolate and estimate the failure bending moment in a random space of three variables wind speed, significant wave height and the load on the wind turbine. Similar methods have been used to find the responses of offshore structures and their probabilities based on the significant wave height, peak period, depth and wind velocity [6–8]. However, use of FORM to estimate the extreme event in a given sea state is more limited. One example is the work of Jensen [9] in which FORM was used to calculate the most probable wave sequence for extreme loads on a jack-up structure, the roll response of a ship and the motion of a TLP floater. Validation of these responses with experiments, however, was not included in this study.

In the present work, FORM is used systematically to estimate extreme wave events that produces large crest heights and large peaks of the inline force, respectively. Strict first- and second-order formulations for wave kinematics and slender body force are applied in 2D and 3D sea states. The NewForce is defined as the force equivalent of the NewWave and the FORM implementation is validated against these theories. The results of FORM are also compared to the designer wave (wave averaged measurements) of the same criteria (same maximum crest height or maximum inline force). The work enables prediction of extreme wave episodes for given free surface and inline force level. The effect of directional spreading can be investigated using results of FORM with a second-order failure function and compared with the measurements. The approach can be generalized to fully nonlinear models.

The experiments were conducted as part of the DeRisk project [10]. Experimentally based analysis of probability curves for crest heights and inline peak force is presented in Schløer et al [11] along with averaged time histories of the corresponding η and force variation. In the last section the results are discussed in a broader view.

2. First Order Reliability Method

Reliability is defined as the probability of a failure function, $g(\mathbf{X})$, being larger than zero where $\mathbf{X}$ is a vector of stochastic input variables. The First Order Reliability Method (FORM) uses a first order Taylor expansion to find the shortest distance between the failure surface (where $g(\mathbf{X})$ is zero) and center of the joint probability distribution of the input variables, mapped to a normalized Gaussian distribution. In other words, FORM provides the most probable combination of the stochastic inputs that lead to failure and the associated probability of its occurrence. The method can be used for structural reliability analysis and for extreme value prediction [9].

In the current paper, four different failure functions are used to predict realization of the most probable time histories for a given peak value of free surface elevation and inline force, for linear and second-order slender body wave loads on a pile.

In equations 1 to 4 the four failure functions and their representation in the next sections are shown.

$$\begin{aligned} \eta^{(1)} &= \sum_{j=1}^{N_{freq}} \sum_{i=1}^{N_{dir}} (a_{ij}\cos(\omega_j t) + b_{ij}\sin(\omega_j t)) \\ g &= \eta_{target} - \eta^{(1)} \\ \text{Represented by} &: FORM(\eta_1) \end{aligned} \tag{1}$$

$$\begin{aligned}
\eta^{(2)} &= \tfrac{1}{4}\sum_{i=1}^{N_{freq}}\sum_{j=1}^{N_{freq}}\cdots \\
&\quad \sum_{k=1}^{N_{dir}}\sum_{l=1}^{N_{dir}}\cdots \\
&\quad (a_{ik}+ib_{ik})(a_{jl}+ib_{jl})\{\{C^{-}_{ijkl}\}\cos(\omega_i t-\omega_j t)+\{C^{+}_{ijkl}\}\cos(\omega_i t+\omega_j t)\} \\
g &= \eta_{target}-(\eta^{(1)}+\eta^{(2)}) \\
\text{Represented by} &: FORM(\eta_1+\eta_2)
\end{aligned} \tag{2}$$

$$\begin{aligned}
F^{(1)} &= \rho A C_M \int_{-h}^{0} u_t^{(1)} dz \\
g &= F_{target}-F^{(1)} \\
\text{Represented by} &: FORM(F_1)
\end{aligned} \tag{3}$$

$$\begin{aligned}
F^{(2)} &= \rho A C_M \int_{-h}^{0} u_t^{(2)}+u^{(1)}u_x^{(1)}+w^{(1)}u_z^{(1)}dz+ \\
&\quad \rho A C_m \int_{-h}^{0} u^{(1)}w_z^{(1)}dz+ \\
&\quad 0.5\rho D C_D \int_{-h}^{0} u^{(1)}|u^{(1)}|dz+ \\
&\quad \rho A C_M \eta u_t^{(1)}|_{z=0} \\
g &= F_{target}-(F^{(1)}+F^{(2)}) \\
\text{Represented by} &: FORM(F_1+F_2)
\end{aligned} \tag{4}$$

where [9]:

$$(a_{i,j}, b_{i,j}) \in \mathcal{N}(0, \sqrt{S\Delta f\Delta\theta}) \tag{5}$$

Further S is the power spectrum of the free surface elevation as a function of frequency and direction. The frequency range was chosen from zero to 2.5 Hz for the present analysis in lab scale, corresponding to 0.35 Hz in full scale. The horizontal particle velocity is denoted by u and u_t is its Eulerian time derivative. The first-order contribution, $u^{(1)}$, is carried out with the Airy Wave theory (1895) while the second-order contribution, $u^{(2)}$, is calculated as by Sharma and Dean [12]. The transfer functions $C^{\pm}$ can be found in the same paper. The force model chosen is the Rainey force model [13] which includes the convective terms of the horizontal particle acceleration and the axial divergence force, as represented in the integrals of (4). In the current implementation of FORM the results of the application are the random variables $a_{i,j}$ and $b_{i,j}$. These known amplitude variables can later be used to reproduce the free surface elevation and inline force time series. We have here chosen to formulate $\eta^{(1)}$ and $F^{(1)}$ as strictly linear and $\eta^{(2)}$ and $F^{(2)}$ as strictly second order. Inclusion of higher-order terms is indeed possible, for example by application of fully nonlinear kinematics which is our next step.

The target values of η_{target} and F_{target} were chosen such that the result could be compared to averaged results of the experiments. However, for a few cases where the effect of slamming was clearly visible in the averaged experimental data, F_{target} was chosen as an estimated non-slamming value, since slamming is beyond the scope of second-order theory.

The Matlab toolbox CODES [14] was used to apply FORM on the chosen failure functions. The sequential quadratic programming (SQP) method was used to find the most probable point on the failure surface. A tolerance value of 10^{-4} was chosen as the convergence criteria. Vectors of zero were used as the initial values for the parameters while it was observed that the results do not depend on the initial values. The code needed approximately 1800 iterations for the most complicated case with directional spreading and second-order effects to converge.

3. NewWave and NewForce theories

The NewWave theory [2] expresses the expected and most likely time history for the linearized free surface elevation around a given crest value, based on its power spectrum $S_\eta(\omega,\theta)$ and the crest height α_η. Application of FORM to

a linear description of the free surface elevation answers the exact same question, and the results of FORM(η_1) must therefore be identical to a NewWave time history. This serves as a check of the FORM application. We here further introduce the NewForce model (see also Schløer et al [11]) as the equivalent theory for the inline force, to express the most likely linear wave episode that produces a specified force peak.

The NewWave free surface elevation for a crest of height α_η in a directionally spread sea state can be written as

$$\eta_{\text{NewWave}}(\mathbf{X},\tau) = \frac{\alpha_\eta}{\sigma_\eta^2}\sum_n\sum_m \text{Re}\left\{d_{n,m}\exp\left(\text{i}(\mathbf{k}_{n,m}\cdot\mathbf{X}-\omega_n\tau)\right)\right\} \tag{6}$$

where

$$d_{n,m} = S_\eta(\omega_n)\Delta\omega_n\Delta\theta_m \tag{7}$$

and $\mathbf{k}_{n,m}$ is the linear wave number vector. Further,

$$\mathbf{X} = \mathbf{x} - \mathbf{x}_0 \tag{8}$$

where $\mathbf{x}_0$ is the focus location and

$$\sigma_\eta^2 = \overline{\eta^2} = \int_{\theta=0}^{2\pi}\int_{\omega=0}^{\infty} S_\eta(\omega_n,\theta_m)\text{d}\omega\ \text{d}\theta. \tag{9}$$

The corresponding linear force time history for an inertia-driven structure can be obtained by application of the Morison equation and integration from the sea bed to the still water level. We may express this through the force transfer function $\Gamma(\omega,\theta)$

$$\Gamma(\omega,\theta) = \text{i}\rho\pi R^2 C_M\cos(\theta)\omega^2/k \tag{10}$$

where k is the wave number, such that

$$F_{\text{NewWave}}(\mathbf{X},\tau) = \frac{\alpha_\eta}{\sigma_\eta^2}\sum_n\sum_m \text{Re}\left\{d_{n,m}\Gamma(\omega_n,\theta_m)\exp\left(\text{i}(\mathbf{k}_{n,m}\cdot\mathbf{X}-\omega_{n,m}\tau)\right)\right\} \tag{11}$$

Note that the drag force has here been omitted due to its second-order magnitude.

The NewForce theory, introduced in [11], uses the same approach to provide the expected force history around a specified target peak value, given the background spectrum. First, the spectrum for the force in the main wave direction is established as

$$S_F(\omega,\theta) = |\Gamma(\omega_n,\theta_m)|^2 S_\eta \tag{12}$$

and next the NewWave approach is applied to express the expected force time history as the corresponding auto-correlation function

$$F_{\text{NewForce}}(\mathbf{X},\tau) = \frac{\alpha_F}{\sigma_F^2}\sum_m\sum_n \text{Re}\left\{S_F\Delta\omega\Delta\theta\exp\left(\text{i}\left(\mathbf{k}_{n,m}\cdot\mathbf{X}-\omega_n\tau\right)\right)\right\} \tag{13}$$

The corresponding free surface elevation can be obtained by division of the force transfer function

$$\eta_{\text{NewForce}}(\mathbf{X},\tau) = \frac{\alpha_F}{\sigma_F^2}\sum_m\sum_n \text{Re}\left\{\Gamma^*(\omega_n,\theta_m)S_\eta\Delta\omega\Delta\theta\exp\left(\text{i}\left(\mathbf{k}_{n,m}\cdot\mathbf{X}-\omega_n\tau\right)\right)\right\} \tag{14}$$

where $*$ denotes the complex conjugate. Results of the FORM analysis is compared to the NewWave and NewForce theories in the following. For the linear predictions $FORM(\eta_1)$ and $FORM(F_1)$, the results must be identical to those of the linear NewWave and NewForce theories. The comparison thus serves as a cross-validation of the two approaches. For the nonlinear results of $FORM(\eta_1+\eta_2)$ and $FORM(F_1+F_2)$ a comparison was made to the linear NewWave and NewForce results with the the second order terms added. It is part of the papers research to investigate how close these results are to each other.

Table 1: Characteristics of the investigated sea states (full scale values).

Case	h [m]	Hs [m]	Tp [s]	Spread [°]	$\frac{h}{gT_P^2}$	$\frac{H_s}{gT_P^2}$
6	33	9.5	12	22	0.023	0.0067
11	33	9.5	12	0	0.023	0.0067
16	20	6.8	12	22	0.014	0.0048
20	20	5.8	12	0	0.014	0.0041

4. Experiments

The experiments were conducted in the shallow water basin at DHI Denmark at a scale of 1:50 as part of the DeRisk project [10]. The full scale diameter of the monopile was 7 m with water depths of 33 m and 20 m. The monopile was mounted on two force transducers — one at the top and one at the bottom — to measure the in-line force and the bending moment. Wave gauges were installed to measure the free surface elevation of the wave propagation towards the cylinder and around it. The monopile was placed 7.3 m from the wave makers (lab scale). The wave generator consisted of 36 piston wave maker driven with linear wave generation theory [15].

Several distinct random sea states were tested for a duration of between 6 and 70 hours (in full scale) from which four were selected for analysis in the current paper. The four sea states were tested both with and without 3D spreading. The cos^{2s} spreading function was used for this purpose. The same was implemented in the failure functions to define the correct spreading in the case of 3D sea states. Table 1 shows the characteristics of these four tests in full scale measures. The spreading angle is the standard deviation of direction at the peak wave frequency.

The chosen tests where repeated twice with and without the structure in the basin. In the 3D cases the free surface elevation measurements from the wave gauge at the location of the monopile in the no-structure tests was used to find the zero down-crossings of the free surface elevation. In the 2D cases, the zero down-crossings of the free surface elevation was found using measurements from a wave gauge in the same distance from the wave paddles as the monopile placed 0.4 m laterally from the pile center. Then for each wave, the maximum and minimum inline force and crest height were identified. After sorting them based on each parameter the corresponding exceedance probabilities were calculated.

The curves for exceedance probability of free surface elevation were next used to choose four crest height values within each test, see figure 4. At each level, the 9 wave events closest to that level were chosen to produce an averaged time history after normalization with the peak value and centering around the peak. The corresponding force histories were also averaged, using the same time shifts as applied for free surface elevation. Figure 5a shows such averaged time histories of η and force, with the error bars showing the standard deviation from the set of 9 waves. As the averaged time histories are conditioned on a certain crest level, they represent the expected wave and force episodes around a certain crest value and can thus be compared to FORM(η). Next, the procedure was repeated, this time by selection of events after force level. An example of exceedance probability and average time histories can be seen in figures 4 and 5a, respectively. The resulting averaged time series can be compared to FORM(F).

It should be mentioned that the force time series from the experiments were low pass filtered so the effect of the resonance of the force transducers are removed from the time series. The natural frequency of the force transducers was about 3 Hz in lab scale [11].

5. Initial FORM results

To initially validate the model before comparing to the measured wave averaged results, a few validation studies were done. This included a convergence study, comparison to the NewWave [2] and NewForce [11] theories and an investigation of the effect of 3D spreading of the waves.

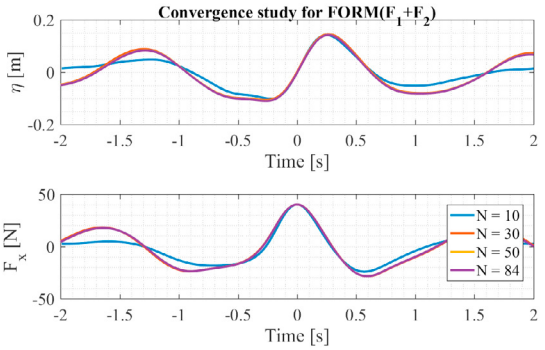

(a) Convergence study of $FORM(F_1+F_2)$ for increasing number of frequency components from 10 to 84.

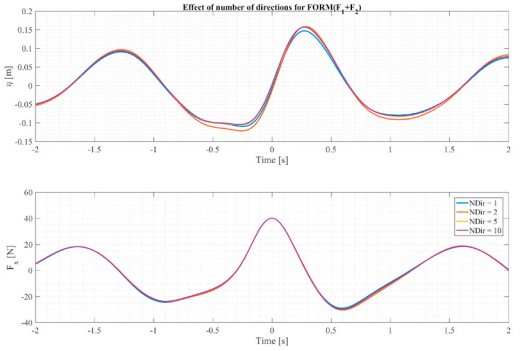

(b) Convergence study of $FORM(F_1+F_2)$ for increasing number of directions from 1 to 10.

Fig. 1: Convergence study of $FORM(F_1 + F_2)$ for increasing number of frequency components and wave directions.

5.1. Convergence study

In calculation of the second order wave quantities, the computation time is directly proportional to $N^2_{freq}N^2_{dir}$. Because of this, a convergence study was performed to estimate the minimum number of frequency components that was needed to approach to an acceptable error level.

In Fig. 1a the results from this study is shown for the case when FORM is minimizing a failure function of first and second order inline force. Based on this figure, the the cases with $N = 30$ frequency components was found to be only marginally different from the highly resolved cases of N = 50 and N = 84. The difference does not exceed 2%. The same behavior was observed for $FORM(\eta_1)$, $FORM(\eta_1 + \eta_2)$ and $FORM(F_1)$. Hence, 30 frequency components were used for all the cases in the current paper. It is expected that a higher number of frequency components is needed for cases that exceed second order-nonlinear effects.

Since, two of the investigated tests in this paper included 3D wave spreading another convergence study was performed to determine the minimum number of directions.

Figure 1b shows the result for this study. It is seen that for a number of directions larger than 5 the difference between the results is marginal and does not exceed 1%. It should be noted that Hence, 5 number of directions was used in the cases that includes directional wave spreading in the experiments.

5.2. Comparison to the NewWave and NewForce theories

The NewWave episode is defined as the most probable and expected shape of an extreme event (in terms of maximum crest height) in a linear random sea state [2]. In addition, the NewForce theory is the equivalent most probable force time series of an extreme event (in terms of maximum inline force) in a linear random sea state [11]. Both of these definitions agree with the definition of the reliability method if used on the respective linear failure functions, see (1) and (3).

To validate the FORM implementation, the result of $FORM(\eta_1)$ and $FORM(F_1)$ are compared with the NewWave and NewForce theories in figure 2a. It can be seen that the shape, amplitude and phases of the time series of free surface elevation and inline force are identical for the results of FORM and the NewWave and NewForce theories. Hereby the FORM implementation is validated.

In figure 2b the result of $FORM(\eta_1 + \eta_2)$ and $FORM(F_1 + F_2)$ are shown in comparison to the time series of NewWave and NewForce including second-order effects. In these figures it can be seen that there are some deviations between the results of FORM and the analytical solutions. This is, however, expected since in the results from both the NewWave and NewForce theories, the theory itself is in the linear domain with subsequent addition of the second order effects, while FORM calculates the most probable combination of frequency components that generate the target extreme value including the second-order contributions. In other words FORM optimizes the combined first-

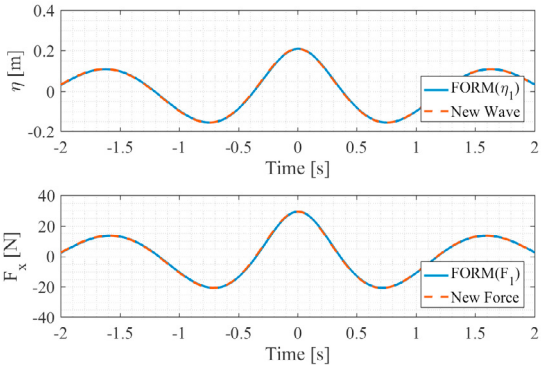

(a) Top: Comparison of free surface elevation time series of NewWave theory and $FORM(\eta_1)$. Bottom: Comparison of inline force time series of NewForce theory and $FORM(F_1)$.

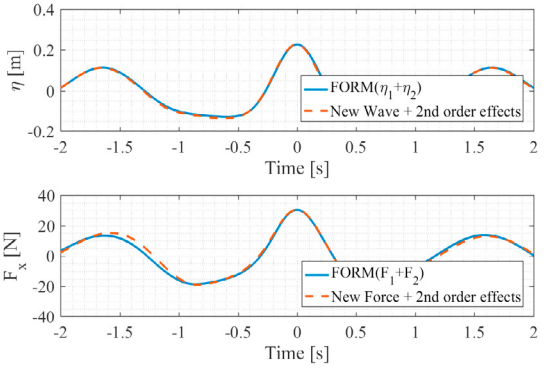

(b) Top: Comparison of free surface elevation time series of NewWave theory including the second order effects and $FORM(\eta_1 + \eta_2)$. Bottom: Comparison of inline force time series of NewForce theory including the second order effects and $FORM(F_1 + F_2)$.

Fig. 2: Comparison of free surface elevation and inline force time series of NewWave and NewForce theory with and without the second order effects.

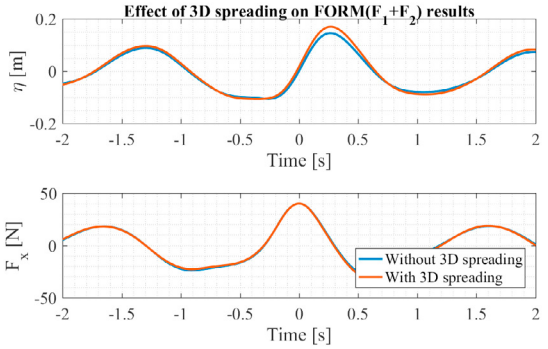

Fig. 3: Free surface elevation and inline force time series comparison of $FORM(F_1 + F_2)$ for cases with and without directional spreading.

and second-order contributions to free surface elevation or inline force, while NewWave provides the solution for an optimization at the linear level.

5.3. Effect of 3D spreading

It is interesting to investigate the difference between a uni-directional and multi-directional random sea state when creating a certain value of inline force. Figure 3 shows this effect through the results of $FORM(F_1 + F_2)$ for a certain target peak inline force with and without directional spreading. The sea state characteristics of cases 006 and 011, from Table 1, are used.

It is seen that the inline force time series is hardly different between the two cases while the corresponding free surface elevation time series show different crest and trough elevations. The wave with the directional spreading has a larger maximum crest height. This is expected because in the calculation of the inline forces the local accelerations should be multiplied by the cosine of the direction of each wave component. Hence to get an equal inline force, the case with directional spreading should contain larger wave amplitudes.

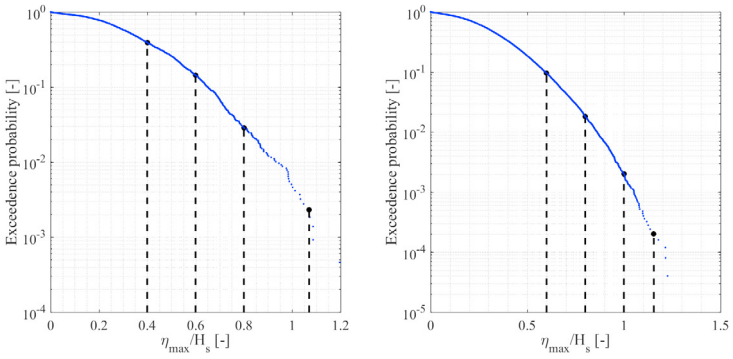

Fig. 4: The exceedance probabilities of maximum crest heights of each wave two sea states. Left: Case 011. Right: Case 006.

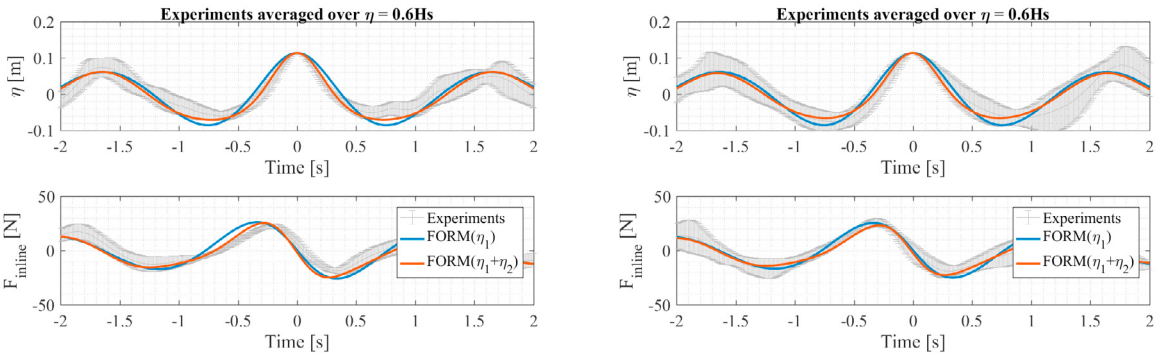

(a) Case 011. (b) Case 006.

Fig. 5: Wave averaged time series of free surface elevation and inline force between 9 waves from case 011 and case 006 with maximum crest height close to $0.6Hs$, in addition to corresponding results from $FORM(\eta_1)$ and $FORM(\eta_1 + \eta_2)$ given $\eta_{target} = 0.6Hs$.

6. Results

In this section the non-dimensional surface elevation and inline force of the selected waves are shown in exceedance probability plots and the wave averaged measurements are compared with the FORM results for selected cases.

6.1. FORM(η) in 33 m water depth

Figure 4 shows the exceedance probability plots of non-dimensional crest heights for sea state cases 011 and 006 which are both in 33 m water depth. The only difference between these two sea states is the directional spreading. This can explain the different maximum crest heights with the same exceedance probability. Since the tests without directional spreading were 6 h long and the ones with directional spreading were 70 h long in full scale, the minimum exceedance probability is one order of magnitude smaller in case 006. The comparison, however, was based on an equal fixed value of non-dimensional crest height ($\eta_{\max}/H_s = 0.6$) so that the directional spreading effect in the experiments and the reproduction of them could be investigated. Four crest heights from extreme to moderate values were chosen for reproduction of the wave shape using FORM.

Figure 5a shows the wave averaged measurements of free surface elevation and the corresponding inline force time series for case 011 in gray colored curves. The standard deviation of η and force between the nine waves is shown with error bars. In the top plot, it can be seen that the error bars are relatively small compared to the amplitude of the main wave itself from the preceding trough to the following one. The same can be seen in the bottom plot for inline

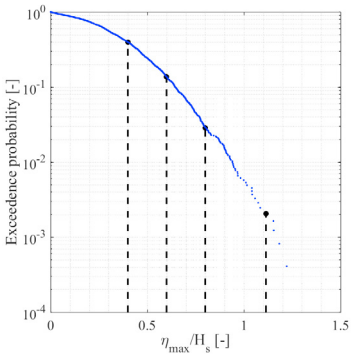

(a) The exceedance probabilities of maximum crest heights of each wave in sea state case 020.

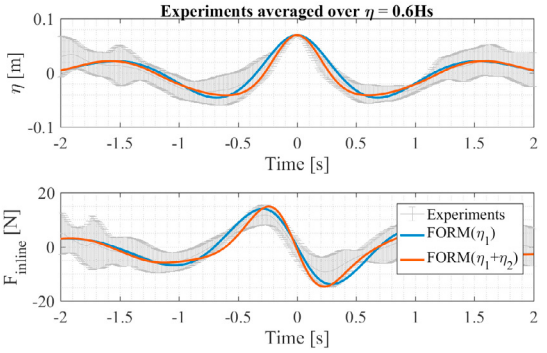

(b) Wave averaged time series of free surface elevation and inline force between 9 waves from case 020 with maximum crest height close to $0.6Hs$, in addition to corresponding results from $FORM(\eta_1)$ and $FORM(\eta_1 + \eta_2)$ given $\eta_{target} = 0.6Hs$.

Fig. 6: The exceedance probabilities of maximum crest height and the wave averaged time series of free surface elevation and inline force.

force. Third harmonic reflections of the waves from the monopile can be seen in the wave averaged time series of free surface elevation as shown and explained in [16] (Figure 3).

In the same figure the results of $FORM(\eta_1)$ and $FORM(\eta_1 + \eta_2)$ and the corresponding calculated inline forces are shown. The linear optimized wave shape, $FORM(\eta_1)$, can hardly predict the general shape of the wave and the inline force time series. While the crest value of η is matched by FORM(η_1) and FORM($\eta_1 + \eta_2$), the amplitude of the linear result is larger than the wave averaged experiments both in free surface elevation and inline force. The result of $FORM(\eta_1 + \eta_2)$ is, however, more in agreement with the experiments. The troughs of the second-order waves are much closer to the experiments compared to the linear FORM results. However, the second-order wave has a wider crest than the measurements with trough amplitude larger than the wave averaged measurements. This shows that the experimental averaged results are more nonlinear than first and second order theories. From the inline force time series, the general shape of the second-order solution is closer to the measurements than for the first order solution. However, marginal differences is seen in the peak and trough amplitude. From the free surface elevation, the FORM results down and up zero crossings have higher slopes than the experiments. Since the free surface elevation and particle acceleration are in phase at least at first order, the larger amplitude of peak and trough of inline force is expected. In the bottom plot also a phase shift between the numerical and experimental results can be seen.

Since the second order numerically reproduced results are in significantly better agreement with the measurements than the first order results the focus will be on the second order results in the following analysis.

To investigate the effect of directional spreading on the expected wave shape of averaged measurements and results of FORM, the similar analysis is shown for case 006 in figure 5b which includes directional spreading.

Based on the free surface elevation comparison of $FORM(\eta_1 + \eta_2)$ to the experiments, the FORM prediction for the shape of the wave is relatively consistent with the measurements. The only significant difference is the asymmetry of η in the measurements which is not captured by the FORM simulations. The same consistency can be seen in the inline force time series. Only marginal differences occur between the measurements and $FORM(\eta_1 + \eta_2)$.

The effect of directional spreading on the measurements of the two presented events, in cases 011 and 006, is investigated. As concluded in section 5.3 with the same inline force the case with directional spreading (here case 006) should have higher maximum free surface elevation than the case without spreading. In other words, waves with the same height in a directional sea state should induce smaller inline force on the monopile. This, however, is not observed in the experiments from figure 5a and 5b. The reason for this inconsistency is part of current research.

6.2. FORM(η) in 20 m water depth

Results for an uni-directional event in 20 m, case 020 are shown in figure 6a. The wave averaged free surface ele-

vation and inline force measurements are shown in gray color curves with error bars presenting the standard deviation between the waves for case 020. The free surface elevation of FORM and corresponding inline force are also shown.

The shape of the free surface elevation of $FORM(\eta_1 + \eta_2)$ compare generally well with the averaged η shape from the measurements. The only significant difference between them is seen in the amplitude of the preceding trough and the slope of the wave from this trough to the main crest. Again $FORM(\eta_1 + \eta_2)$ matches the experimental results better than $FORM(\eta_1)$.

From the bottom plot, the corresponding inline force time series of $FORM(\eta_1 + \eta_2)$ has higher amplitude than the wave averaged measurements. The inline force time series based on $FORM(\eta_1 + \eta_2)$, is inside one standard deviation range of wave averaged experiments. Since H_s is different between the depths of 20 m and 33 m, no direct comparison of the events of figure 6b and 5a is made. From the shape of the curves, however, the force peak at 20 m can be seen to be more compact than at 33 m.

6.3. FORM(F) in 33 m water depth

We now turn to the expected shape of inline force time history, conditional to the force peak value. Figure 7 shows the exceedance probability plots of the non-dimensional inline force peaks for cases 011 and 006. Four target inline force values from extreme to moderate were chosen for each case, to reproduce their wave shape using FORM. Similarly to the expected shape of η, pair-wise common peak force values were also chosen to investigate the spreading effect on the results, in this case $F/\rho g h R^2 = \{1.2, 1.7\}$.

Figure 8a shows the wave averaged measurements of free surface elevation and inline force time series of case 011 together with the FORM results. For the selected force level, the wave events were found to contain slamming, resulting in a relatively sharp peak on top of the smoother underlying force curve. As another indicator of strong nonlinearity, a secondary load cycle can be observed in the trough following the maximum inline force. Since the effect of slamming is beyond the second-order wave and force model, the target peak force in the FORM optimization was chosen to be lower than the maximum of the wave averaged signal. For this reason the resulting inline force time series of $FORM(F_1 + F_2)$ has a peak value smaller than the peak of the averaged force.

Based on comparison of the inline force result of $FORM(F_1 + F_2)$ with the experiments in the lower plot, the amplitude of the inline force is predicted relatively consistently. However, the FORM results inline force time series has a higher preceding slope and lower following slope around the main peak.

In the top plot a phase shift is seen between the numerical and experimental results, similarly to the previous cases. This phase shift was investigated more thoroughly by comparing the results from all of analyzed events and it is presented in section 7. It was observed that the magnitude of this time shift is directly proportional to the target maximum crest height and target peak inline force. The time shift can be linked to the overturning behaviour of near-breaking waves which leads to temporal asymmetry of the crest. The second-order FORM model is able to reproduce some of this asymmetry. In the same plot it is seen that the preceding and the following slope of the free surface elevation generated by $FORM(F_1 + F_2)$ are consistent with the wave averaged experiments. However, the maximum crest height is not captured by the results of $FORM(F_1 + F_2)$. In addition, from the preceding trough of the main peak in the second order free surface elevation time series, it is seen that a small crest is visible in the trough. This indicates the second order theory is not valid to include all the nonlinearity in this case. Hence it can be concluded that the experimental wave includes more nonlinearity than the second order theory. Based on comparison of the exceedance probability of this wave with the one presented in section 6.1 it can be seen that the exceedance probability of the current wave is about 1.5% compared to about 15% in the previous case (case 11, $\eta = 0.6H_s$). Hence the large nonlinearity is expected. Despite higher nonlinearity effects, the reproduced wave by $FORM(F_1 + F_2)$ is in the range of one standard deviation of the wave averaged experiments most of the times.

To investigate the directional spreading effect on the measurements and FORM results of the same wave, results of case 006 is analyzed in the following. In figure 8b, in the bottom plot, the wave averaged inline force time series is seen in gray. Similarly to the 2D case, the effect of slamming is seen at the peak of the time series. Based on comparison of the $FORM(F_1 + F_2)$ inline force time series with the experiments, the amplitude of the time series compares well neglecting the effect of slamming in the crest of the time series around the main peak.

Further, from the top plot, the free surface elevation time series resulting from $FORM(F_1 + F_2)$ have a generally good agreement with the measurements, however, with lower amplitude. Similarly to the equivalent 2D event, the experiments results look more nonlinear than the FORM results.

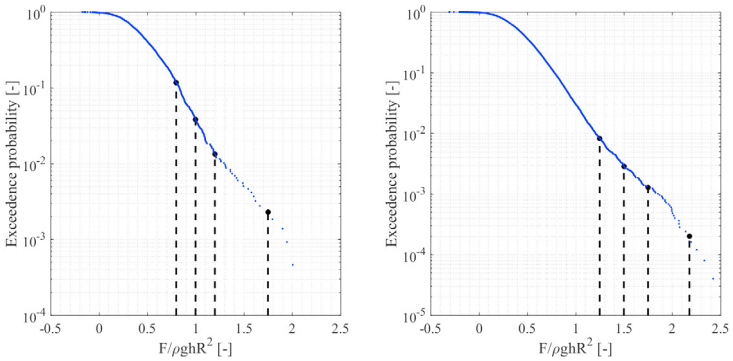

Fig. 7: The exceedance probabilities of maximum inline force of each wave in one sea state cases 011 (left plot) and case 006 (right plot).

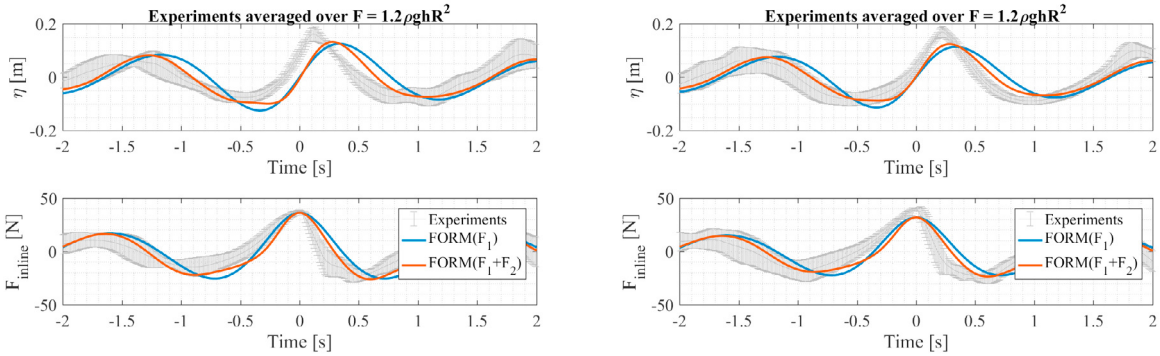

(a) Case 011. (b) Case 006.

Fig. 8: Wave averaged time series of free surface elevation and inline force between 9 waves from case 011 and case 006 with maximum inline force close to $1.2\rho ghR^2$, in addition to corresponding results from $FORM(F_1)$ and $FORM(F_1 + F_2)$ given $F_{target} = 1.2\rho ghR^2$

In figure 8a and 8b similar slamming effect is observed. As concluded in section 5.3 with the same inline force the case with directional spreading (here case 006) should have higher maximum free surface elevation than the case without spreading. This, however, is not observed in the experiments similarly to the previous comparison of the experiments with and without directional spreading in section 6.1.

From figure 8b and figure 5b, the former plots of the wave averaged experiments look more nonlinear. From the corresponding exceedance probability plots, figure 4 and figure 7 it is seen that the exceedance probability of the waves investigated in figure 8b is about 0.8% while it is around 10% for the waves investigated in figure 5b. This explains the larger nonlinearity in the latter case, figure 5b.

6.4. FORM(F) in 20 m water depth

To investigate the effect of water depth, in this section, similar results for an event in 20 m depth are investigated. Figure 9a shows the exceedance probability plot of the non-dimensional inline force peaks of case 016, in 20 m water depth including directional spreading.

In figure 9b, in the bottom plot the inline force time series of case 016 is shown similar to the previous cases. The corresponding free surface elevation is seen in the top plot.

The amplitude of the inline force time series of $FORM(F_1 + F_2)$ is consistent with the wave averaged experiments. However, the preceding slope is slightly larger than the one from the experiments.

From the top plot it can be seen that apart from the time shift between the numerical results and the experiments, the slopes and the amplitude of the waves are consistent. It is seen that the wave of $FORM(F_1 + F_2)$ is beyond the

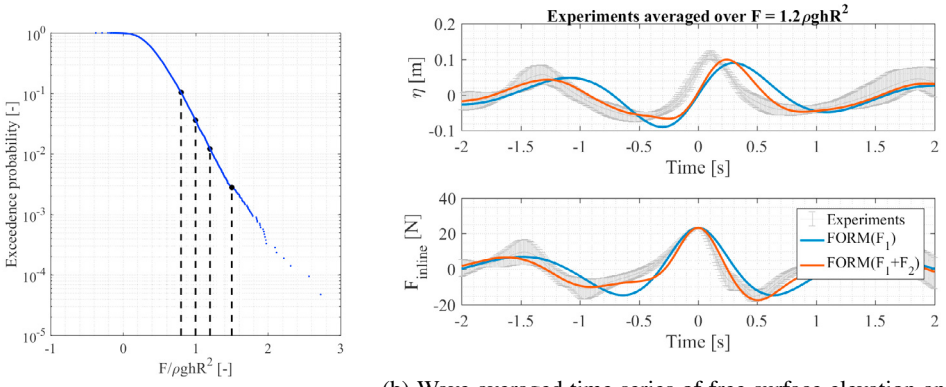

(a) The exceedance probabilities of maximum inline force of each wave in one sea state cases 016.

(b) Wave averaged time series of free surface elevation and inline force between 9 waves from case 016 with maximum inline force close to $1.2\rho ghR^2$, in addition to corresponding results from $FORM(F_1)$ and $FORM(F_1+F_2)$ given $F_{target} = 1.2\rho ghR^2$.

Fig. 9: The exceedance probabilities of maximum inline force and the wave averaged time series of free surface elevation and inline force.

limit of second order theory demonstrated by the small crest inside the preceding trough of the free surface elevation. Also the maximum crest height of the wave averaged measurements is larger than the free surface elevation based on $FORM(F_1 + F_2)$, similar to the previously investigated events.

Based on figure 8b and figure 9b, the event in case 016, with smaller water depth is more nonlinear.

7. Quantification of FORM agreement

Based on the full set of results, more analysis was conducted over the agreement of the model results with the wave averaged measurements in terms of amplitude and phase shift. The analysis also included the standard deviation of the wave averaged measurements. The results are categorized into two groups where in the first group the objective was to find the most probable wave shape given η_{target} while in the second group F_{target} was given.

To quantify the FORM agreement with the measurements, the following definition of relative error measure was applied after shifting the time series to remove the time offset between them

$$E = \frac{\sqrt{\overline{(\mathbf{X} - \mathbf{X}_{\mathbf{measured}})^2}}}{\max(\mathbf{X}_{\mathbf{measured}})} \tag{15}$$

First group with given η_{target}

Figure 10a shows the relative mean error, E, of four test cases, for first and second order free surface elevation and inline force, in relation to the wave averaged measurements. For the free surface elevation of second order FORM results, E is between 6% and 18% in all analyzed events. The average error between the inline force signals of second order FORM results and the measurements, however, was larger and up to 32%. The average error of the first-order results was about twice as large. The smallest agreement was observed between the inline force time series of $FORM(\eta_1)$ and the measurements. The errors for this comparison went up to 44%. The best agreement was seen in free surface elevation comparisons of FORM results $FORM(\eta_1 + \eta_2)$ and the measurements.

No clear relation between the directional spreading and the standard deviation of the measurements was seen when events with the same exceedance probability were chosen with and without spreading.

The time shift between the results from the models and the wave averaged measurements was observed to be directly proportional to the target maximum crest height. Figure 10b shows this effect clearly. The phase shifts between the FORM results and the measurements vary from zero to one radian. The phase shifts of the first order

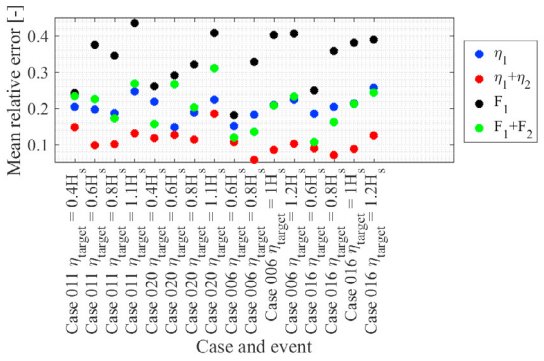

(a) The mean relative error of free surface elevation and inline force time series including first and second order for the cases with known η_{target}.

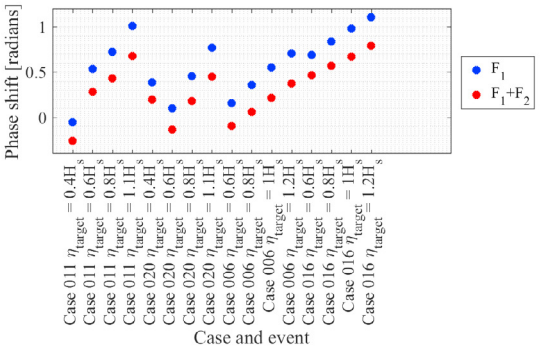

(b) The phase shift of inline force time series including first and second order for the cases with known η_{target}.

Fig. 10: The mean relative error of $FORM(\eta)$ results and the phase shift of the force time series.

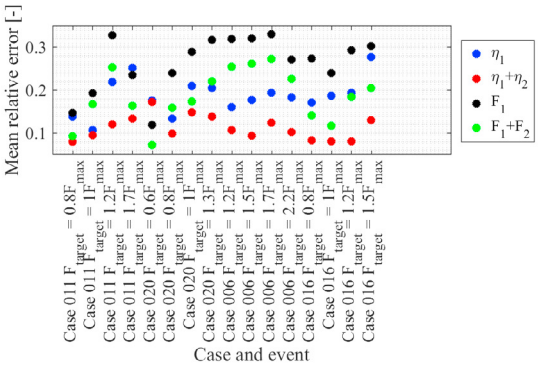

Fig. 11: The mean relative error of free surface elevation and inline force time series including first and second order for the cases with known F_{target}.

FORM results are about 0.3 radian higher than the second order included results. This could be related to the fact that to keep the inline force calculation strictly second order, the drag term in the Morison equation was only calculated up the still water level. This means that for the times that the waves are at the highest elevation, with highest horizontal velocity, a large drag contribution to the inline force is neglected.

Second group with given F_{target}

Figure 11 shows E of the same four time series, as in figure 10a, with given F_{target}. Similarly to the results given η_{target}, in general the agreement of FORM results and the wave averaged measurements for free surface elevation time series are in better agreement than the inline force time series. The relative mean error for free surface elevation of second order FORM is less than 11%. The error for the first order FORM is about 1.5 times as big as the second order included FORM for both free surface elevation and inline force time series.

Similarly to the previous group of results, the best agreement is in free surface elevation comparisons of FORM results and the measurements.

The same magnitude and behavior of the phase shifts as for the first group was observed for the second group of results.

8. Summary and discussion

FORM was used to predict the extreme wave episodes defined by maximum crest height and maximum inline force in 2D and 3D sea states. The NewForce model was defined as the force equivalent of the NewWave and the FORM implementation was validated against both theories. The results were linearly consistent. Further the results of FORM for a second-order target was found to have only minor deviations to the curves obtained as first-order NewForce with the second-order terms added. The results of FORM were also compared to the wave averaged measurements of the same target crest height or inline force.

In summary, it was observed that the events with larger target crest height or peak inline force values, had smaller deviations relative to the averaged signal of 9 waves. This is in agreement with the NewWave theory.

Generally, a relatively good agreement between the First Order Reliability Method results and the wave averaged measurements was observed. The agreement was further increased by adding the second-order terms into the target of the FORM analysis, leading to a better reproduction of the asymmetry around the force peak value. In addition, it was seen that the relative error between the reproduced second-order free surface elevation and the measurements was larger for larger (more nonlinear) target values with lower exceedance probability. It is expected that with a more nonlinear model a better agreement between the FORM results and the measurements is possible.

Larger deviations were observed between FORM and measurements where seen for the inline force than for the free surface elevation. This can be explained by the omission of the drag terms above still water level. Here a more nonlinear force model, can expectedly reduce this discrepancy. The inclusion of the drag term above still water level and higher-order nonlinearity can also reduce the phase errors between the FORM results and the measurements. This is part of current research to use FORM together with the fully nonlinear potential flow solver, OceanWave3D [17], so that all the nonlinear effects are included up to the free surface level.

It was observed that FORM predicts larger crest height for the same target inline force peak value in the multi-directional sea than in the unidirectional sea. This was not observed in the measurements. This inconsistency may be explained by presence of slamming inline forces and effects beyond the second-order model accuracy. This aspect is subject to further work. It is envisaged that such further imporovements will lead to more accurate design waves for offshore wind turbine substructures.

9. Acknowledgement

The present research was partly funded by the DeRisk project of Innovation Fund Denmark, grant number 4106-00038B. Further funding was provided by Statoil and the participating partners. All funding is gratefully acknowledged. Prof. Paul H. Taylor, Dr. Thomas A. A. Adcock and Dr. Dripta Sarkar, University of Oxford, are gratefully thanked for stimulating discussions.

References

[1] Dean, R.G.. Stream function representation of nonlinear ocean waves. Journal of Geophysical Research 1965;70(18):4561–4572.
[2] Tromans, P.S., Anatruk, A.R., Hagemeijer, P.. New Model for the Kinematics of Large Ocean Waves Application as a Design Wave. Proceedings of the First International Offshore and Polar Engineering Conference 1991;8(August):64–71.
[3] En, D.S.. Dansk standard Elproducerende vindmøller Del 3 : Konstruktionskrav til offshorevindmøller 61400-3 2009;.
[4] Grice, J.R., Taylor, P.H., Taylor, R.E.. Second-order statistics and designer ' waves for violent free-surface motion around multi-column structures Subject Areas : 2014;.
[5] Agarwal, P., Manuel, L.. Wave Models for Offshore Wind Turbines. 46th AIAA Aerospace Sciences Meeting and Exhibit 2008;(January):15.
[6] Eckert-gallup, A.C., Sallaberry, C.J., Dallman, A.R., Neary, V.S.. Modified Inverse First Order Reliability Method (I-FORM) for Predicting Extreme Sea States. Sandia National Laboratories Report 2014;(September):41.
[7] Valamanesh, V., Myers, A.T., Arwade, S.R.. Multivariate analysis of extreme metocean conditions for offshore wind turbines 2015;55:60–69.
[8] Ewans, K., Jonathan, P.. Evaluating environmental joint extremes for the offshore industry using the conditional extremes model. Journal of Marine Systems 2014;130(November 2012):124–130.
[9] Jensen, J.J.. Extreme value predictions and critical wave episodes for marine structures by FORM. Ships and Offshore Structures 2008;3(4):325–333.
[10] Bredmose, H., Dixen, M., Ghadirian, A.. DeRisk - Accurate prediction of ULS wave loads. Outlook and first results. 2016,.
[11] Schløer, S., Bredmose, H.. Analysis of experimental data: The average shape of extreme wave forces on monopile foundations. In: DeepWind. 2017,.

[12] Sharma, J.N., Dean, R.G.. Second-Order Directional Seas and Associated Wave Forces. Society of Petroleum Engineers journal 1981;21(1):129–140.
[13] Rainey, R.C.T.. Slender-body expressions for the wave load on offshore structures. Proceedings of the Royal Society of London 1995;450(1939):391–416.
[14] Lacaze, S., Missoum, S.. No Title. 2015.
[15] Dean, R.. Water wave mechanics for engineers and scientists; vol. 53. 2013.
[16] Ghadirian, A., Bredmose, H., Dixen, M.. Breaking phase focused wave group loads on offshore wind turbine monopiles. Journal of Physics: Conference Series 2016;753:092004.
[17] Engsig-Karup, a.P., Bingham, H.B., Lindberg, O.. An efficient flexible-order model for 3D nonlinear water waves. Journal of Computational Physics 2009;228(6):2100–2118.